Carbon 260 (2026) 121956

Contents lists available at ScienceDirect

Carbon

journal homepage: www.elsevier.com/locate/carbon

Research paper

Distinction between inelastic scattering and dephasing exponents by current heating in gated epitaxial graphene

Wei-Chen Lin [a], Po-Shao Lai [a], Sung-Chieh Chiu [a], Pin-Chi Liao [a], Fa-Hua Chen [a], Ji-Song Hsu [a], Ying-Je Wu [a], Kenji Watanabe [b], Takashi Taniguchi [c], Shao-Yu Chen [d,e,f], Albert F. Rigosi [g], Yanfei Yang [g], Chi-Te Liang [a,h,i,j,*]

[a] Department of Physics, National Taiwan University, Taipei 106, Taiwan
[b] Research Center for Electronic and Optical Materials, National Institute for Materials Science, Tsukuba 305-0044, Japan
[c] Research Center for Materials Nanoarchitectonics, National Institute for Materials Science, Tsukuba 305-0044, Japan
[d] Center for Condensed Matter Sciences, National Taiwan University, Taipei 106, Taiwan
[e] Center of Atomic Initiative for New Materials, National Taiwan University, Taipei 106, Taiwan
[f] Institute of Physics, National Yang Ming Chiao Tung University, Hsinchu 300, Taiwan
[g] Physical Measurement Laboratory, National Institute of Standards and Technology (NIST), Gaithersburg, MD 20899, USA
[h] Taiwan Semiconductor Research Institute (TSRI), Hsinchu 300, Taiwan
[i] Center for Quantum Science and Engineering (CQSE), National Taiwan University, Taipei 106, Taiwan
[j] Taiwan Consortium of Emergent Crystalline Materials (TCECM), Taipei 106, Taiwan

ARTICLE INFO

Keywords:
Graphene
Electron heating
Inelastic scattering
Dephasing
SiC

ABSTRACT

The interplay of electron–electron (e–e) scattering and electron–phonon (e–p) scattering plays a crucial role in dephasing in quantum transport. To identify the dominant scattering mechanism, the inelastic scattering exponent p and the dephasing exponent p' become essential. Prior studies have suggested an equivalence between p, extracted from the inelastic scattering length L_{in}, and p', obtained from the dephasing length L_{ϕ}. Here, in epitaxial graphene on SiC, we report a pronounced discrepancy between $p \approx 2$ and $p' \approx 1$ when the applied gate voltage V_G is 0. With increasing V_G, the contrasting evolution of p and p' demonstrates stronger evidence that they are not universally equivalent. These findings reveal that the commonly assumed correspondence between p (from ≈ 2 to ≈ 3) and p' (from ≈ 1 to ≈ 0.75) is not valid beyond a limited current range and with different carrier densities, offering new insight into scattering mechanisms in two-dimensional systems.

1. Introduction

At sufficiently low temperatures, where phonon activity is strongly suppressed, electron–phonon (e–p) coupling becomes weak and results in an extreme thermal isolation property of graphene [1–4]. This indicates that electron–electron (e–e) interactions, arising from Coulomb interactions between electrons [5], becomes the dominant energy exchange mechanism. The inelastic scattering length L_{in} represents the relaxation of the energy distribution toward thermal equilibrium [6]. The scaling behavior of L_{in} is given by [7–10]

$$L_{in} \sim T^{-p/2}, \tag{1}$$

where p is the inelastic scattering exponent and T is the temperature.

Through current-heating experiments, electrons possess a distinct effective temperature T_{eff} from the lattice temperature. The relation between the applied current I and T_{eff} is given by [10–14]

$$T_{eff} \sim I^{\alpha}, \tag{2}$$

where α is the current heating exponent. The thermal energy that the electron acquired is expressed as [10,11]

$$k_B T_{eff} \sim eEL_{in}, \tag{3}$$

where k_B is the Boltzmann constant, e is the elementary charge, and E is the electric field. By substituting Eqs. (2) and (3) in Eq. (1), the relation between p and T_{eff} can be written as [10,11]

$$T_{eff} \sim I^{2/(2+p)}. \tag{4}$$

In general, a value of $p = 2$ is typically associated with e–e interactions governed by energy dissipation in a diffusive two-dimensional Fermi

* Corresponding author at: Department of Physics, National Taiwan University, Taipei 106, Taiwan.
E-mail address: ctliang@phys.ntu.edu.tw (C.-T. Liang).

https://doi.org/10.1016/j.carbon.2026.121956
Received 11 June 2026; Received in revised form 27 July 2026; Accepted 1 August 2026
Available online 16 August 2026

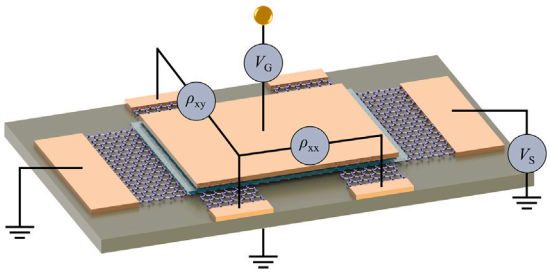

Fig. 1. Cartoon of the four-terminal measurements on an epitaxial graphene QHD. The longitudinal resistivity ρ_{xx} was obtained from the measured longitudinal resistance R_{xx} using $\rho_{xx} = R_{xx} \times W/L$, where W is the Hall-bar width and L is the distance between the longitudinal voltage probes. The Hall resistivity was taken as $\rho_{xy} = R_{xy}$.

liquid [10,15]. The observed increase in p is consistent with values reported in previous studies where e–p scattering plays an increasingly important role. [7,16].

The dephasing length L_ϕ quantifies the extent to which electrons maintain quantum phase coherence [6] and follows a temperature dependence given by $L_\phi \sim T^{-p'/2}$ (Ref. [17–19]), where p' is the dephasing exponent that identifies the dominant scattering mechanism depending on the system dimensionality and the film quality [18,20]. In two dimensions, the nature of e–e scattering leads to different dephasing behaviors and results in a distinct value of p'. In the dirty limit regime, where electron motion is diffusive, dephasing is governed by Nyquist scattering, which originates from interactions with dynamically fluctuating electromagnetic potentials generated by surrounding electrons [20]. This low-energy-transfer process results in a linear temperature dependence of the dephasing rate, $1/\tau_\phi \sim T$, yielding $p' = 1$ (Ref. [21–25]). In contrast, in the clean limit regime, where carriers enter the ballistic regime, dephasing is dominated by large-energy-transfer e–e scattering processes. These processes are more efficient in relaxing phase coherence and lead to a quadratic temperature dependence, $1/\tau_\phi \sim T^2$, corresponding to $p' = 2$ (Ref. [25]).

Seminal studies have shown that L_{in} is generally comparable to L_ϕ when e–e scattering dominates under finite environmental (lattice) temperatures [11,12,26–30]. Consequently, the exponent p, extracted from L_{in}, has often been considered equivalent to p' obtained from L_ϕ. However, our previous work revealed a clear discrepancy between $p \approx 2$ and $p' \approx 1$, even under a finite lattice temperature, which might originate from the breakdown of the equilibrium between e–e and e–p scatterings [31].

Here, we provide further evidence that p and p' are not universally equivalent, as the discrepancy manifests not only in their values but also in their distinct evolution with increasing gate voltage V_G. While p increases from ≈ 2 to ≈ 3, indicating a clear crossover from e–e to e–p scattering [7,16], p' instead exhibits a contrasting decreasing monotonic evolution from ≈ 1 to ≈ 0.75 within the measured gate-voltage range.

2. Experimental details

The monolayer epitaxial graphene quantum Hall device (QHD), grown on a 4H-SiC(0001) substrate [32], was functionalized with chromium tricarbonyl [$Cr(CO)_3$] to shift the Fermi level closer to the Dirac point and to provide additional stability [33]. Following a standard photolithography technique, which provides guaranteed high-quality and reproducibility epitaxial graphene [34–37], the investigated device was etched into a Hall bar geometry with a length of 40 μm and a width of 5 μm. A hexagonal boron nitride (h-BN) flake, with a thickness of approximately 60 nm, was subsequently transferred onto the graphene surface to serve as the dielectric layer, followed by a deposition of a 50-nm-thick Au/Pt top gate. The experiment was carried out with standard four-terminal measurements, as illustrated in Fig. 1. At $V_G = 0$ V, the carrier density and mobility are estimated to be 2.3×10^{11} cm^{-2} and 4970 cm^{2}V^{-1}s^{-1}, respectively.

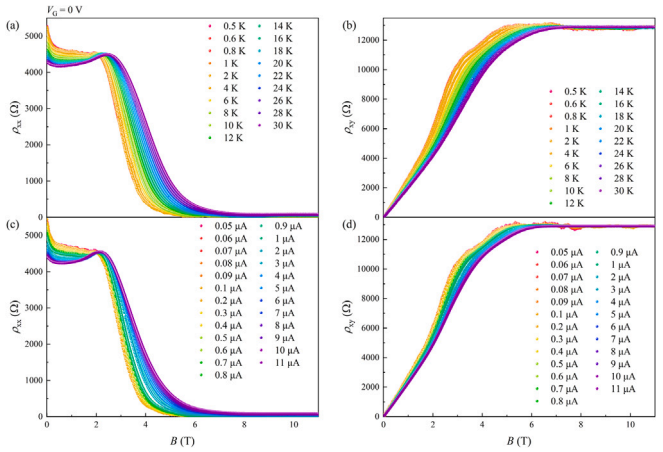

Fig. 2. Magnetotransport measurements of the QHD at $V_G = 0$ V. (a) Temperature-dependent longitudinal resistivity ρ_{xx} and (b) Hall resistivity ρ_{xy} ranging from 500 mK to 30 K with an applied current $I = 0.1$ μA. (c) Current-dependent ρ_{xx} and (d) ρ_{xy} with different applied current from 0.05 μA to 11 μA at T_{base}.

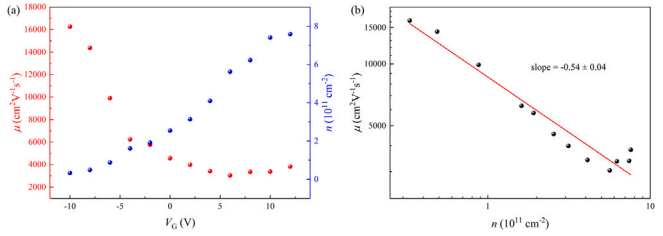

Fig. 3. Characteristics of the QHD. (a) Schematic of V_G-dependent μ (red data) and n (blue data) from $V_G = -10$ V to 12 V. (b) Illustration of μ plotted against n on a double-logarithmic scale. The linear fit (red line) shows a correspondence of nearly $\mu \sim n^{-1/2}$. (For interpretation of the references to color in this figure legend, the reader is referred to the web version of this article.)

3. Results

Fig. 2 presents the magnetotransport characteristics of the QHD at $V_G = 0$ V, showing both the longitudinal resistivity ρ_{xx} and the Hall resistivity ρ_{xy} after symmetrization and antisymmetrization, respectively. Data at higher gate voltages ($V_G = 2$, 4, and 8 V) are provided in Supplementary Section [38]. Notably, both ρ_{xx} (Fig. 2c) and ρ_{xy} (Fig. 2d) remain unchanged at $I < 0.4$ μA, indicating negligible electron heating in this regime.

The carrier density n, shown as the blue data in Fig. 3a, is extracted from the slope R_H of ρ_{xy} (Fig. 2b) within a small magnetic field (−0.5 T to 0.5 T), via $n = 1/(eR_H)$, where e is the elementary charge. The mobility μ (red points depicted in Fig. 3a) is calculated via the relation given by $\mu = R_H/\rho_{xx0}$, where ρ_{xx0} is the zero-field resistivity shown in Fig. 2a. The relation between n and μ follows a power-law behavior, written as $\mu \sim n^{-1/2}$, shown as the linear fit in Fig. 3b, which is consistent with prior studies [39–41].

3.1. Extraction of the inelastic scattering exponent p

The two-bath model, in which e–e scattering and e–p scattering are treated as two separate thermal reservoirs, provides an alternative to

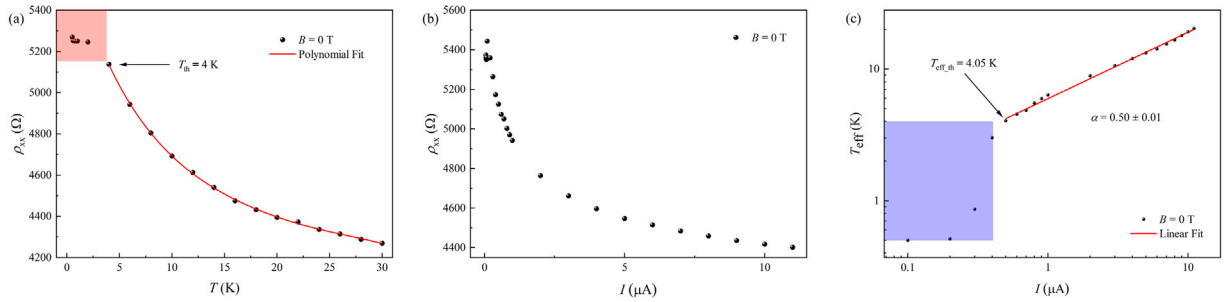

Fig. 4. The extraction of T_{eff} at $B = 0$ T. (a) Temperature-dependent ρ_{xx}. The red region indicates a temperature-independent regime, where ρ_{xx} remains nearly constant. The arrow indicates a threshold temperature ($T_{\mathrm{th}} = 4$ K) that could be guaranteed for T_{eff} estimation. The red curve shows a fifth-order polynomial fit to the data points. (b) Current-dependent ρ_{xx}. (c) Schematic of T_{eff} as a function of I at zero magnetic field ($B = 0$ T) on a double-logarithmic scale. The blue region ($T_{\mathrm{eff}} < 4$ K) shows a forbidden area where T_{eff} estimation is unavailable, owing to the insufficient electron heating (shown as the red area in Fig. 4a). In the high-current regime, the red line represents a linear fit, from which the slope gives the exponent $\alpha = 0.50 \pm 0.01$. The arrow points out $T_{\mathrm{eff_th}} = 4.05$K (corresponding to ≈ 0.5 μA), marking the lower bound of the fitting range. (For interpretation of the references to color in this figure legend, the reader is referred to the web version of this article.)

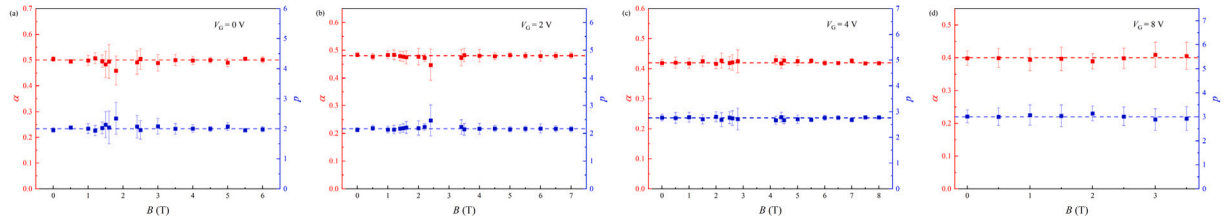

Fig. 5. Exponents α (red) and p (blue) plotted against B at (a) $V_{\mathrm{G}} = 0$ V, (b) $V_{\mathrm{G}} = 2$ V, (c) $V_{\mathrm{G}} = 4$ V, and (d) $V_{\mathrm{G}} = 8$ V. A gradual decrease and increase are exhibited in α and p, respectively, with increasing V_{G}. Error bars are the standard deviation (1σ) obtained from the linear fitting. (For interpretation of the references to color in this figure legend, the reader is referred to the web version of this article.)

determining the exponents α and p [12]. The close resemblance between the temperature-dependent (Fig. 4a) and the current-dependent (Fig. 4b) ρ_{xx} provides an approach to determine the effective temperature T_{eff} for each applied current while the lattice maintained at a finite base temperature $T_{\mathrm{base}} = 500$ mK, as shown in Fig. 4c. Notably, the blue region ($T_{\mathrm{eff}} < 4$ K) indicates that the T_{eff} estimation becomes unreliable owing to the temperature-independent ρ_{xx} in the low-temperature regime (illustrated as the red region in Fig. 4a), suggesting that the injected power is insufficient to overcome energy relaxation via *e–p* scattering. This undistinguishable T_{eff} region shows great agreement with the overlapped ρ_{xx} and ρ_{xy}, as illustrated in Fig. 2. In this low-current regime, the system may remain close to thermal equilibrium with the lattice, and electron heating is negligible. In other words, *e–e* and *e–p* scattering processes are effectively balanced, maintaining the system in an equilibrium state.

To quantify the current-induced T_{eff}, a fifth-order polynomial fit was applied to the temperature-dependent ρ_{xx}, shown as the red curve in Fig. 4a. The current-dependent ρ_{xx}, shown in Fig. 4b, was then converted into T_{eff} by substituting each ρ_{xx} value into the fitted polynomial. The resulting current dependence of T_{eff} is shown in Fig. 4c.

A linear fit to the high-current regime ($I \geq 0.5$ μA), shown as the red line in Fig. 4c, follows Eq. (2) and yields $\alpha = 0.50 \pm 0.01$, which shows great agreement with seminal studies [10,31]. Within the framework of the current heating model, α can be directly linked to the exponent p through the scaling relation given by $\alpha = 2/(2+p)$ (Ref. [11]), and yields $p = 2.00 \pm 0.08$. A value of $p \approx 2$ is expected for the *e–e* scattering in the diffusive regime of two-dimensional systems, which is consistent with prior studies in graphene [19,31] and GaAs systems [42,43]. Notably, both α and p show no discernible dependence on the magnetic field B, as depicted in Fig. 5a, which is consistent with prior studies [31,44]. This independence from B indicates that *e–e* interactions govern the dominant energy relaxation process at high currents. Moreover, in this high-current regime, current-induced hot carriers drive the system out of equilibrium, as the energy dissipation through *e–p* interactions remains mostly unchanged, while the energy exchange among electrons increases via *e–e* scattering [31]. This interpretation is consistent with earlier studies in GaAs systems [42,43], showing that current heating does not significantly affect the inelastic scattering process, but solely influence the dephasing mechanism.

With increasing V_{G}, α gradually decreases from 0.5 to 0.4 while p increases from 2 to 3 (Fig. 5), indicating a transition of the temperature dependence of the energy relaxation power [14]. This evolution suggests a crossover of the dominant scattering mechanism from *e–e* to *e–p* scattering [7,16]. Such a transition demonstrates that the enhanced *e–p* coupling at higher carrier densities with increasing V_G, as shown in Fig. 3a, raises the efficiency of the energy dissipation to the lattice. For more information regarding the exponents α and p at $V_{\mathrm{G}} = 8$ V, please see the Supplementary Section [38].

3.2. Extraction of the dephasing exponent p'

The temperature-dependent L_ϕ allows extraction of the exponent p' and provides insight into the dominant scattering mechanism. At $B \leq 0.2$ T, the converted magnetoconductivity $\Delta\sigma_{\mathrm{xx}} = \sigma_{\mathrm{xx}}(B) - \sigma_{\mathrm{xx}}(B = 0)$ exhibits a pronounced signature of the weak localization (WL) effect, which gradually diminishes with increasing temperature, as depicted in Fig. 6a–d. To quantitatively analyze the WL effect, we employ the Hikami–Larkin–Nagaoka (HLN) model, given by [45,46]:

$$\Delta\sigma_{xx}(B) = \frac{e^2}{\pi h}\left[F\left(\frac{B}{B_\phi}\right) - F\left(\frac{B}{B_\phi + 2B_i}\right) - 2F\left(\frac{B}{B_\phi + B_i + B_*}\right)\right], \tag{5}$$

where $B_\phi = \frac{h}{8\pi e L_\phi^2}$, $B_i = \frac{h}{8\pi e L_i^2}$, $B_* = \frac{h}{8\pi e L_*^2}$, L_i, and L_* are intervalley and intravalley scattering lengths, respectively. The notation $F(z) = \ln z + \Psi(0.5 + z^{-1})$ and $\Psi(x)$ is the digamma function.

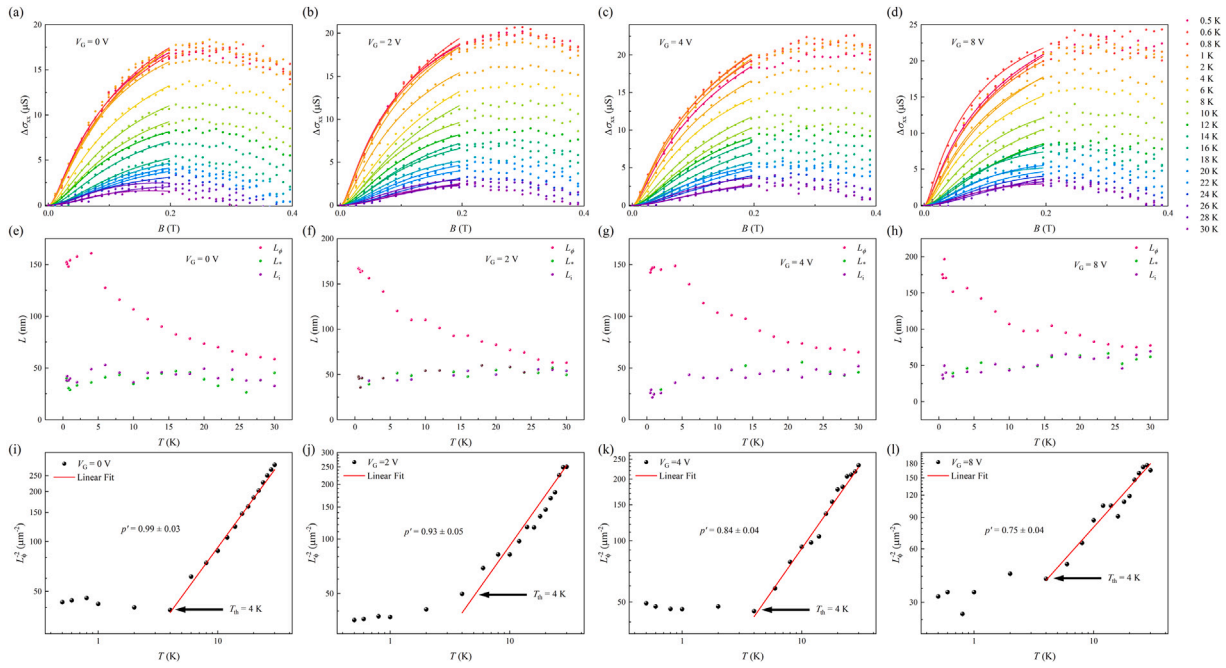

Fig. 6. Characteristics of the WL effect at $V_G = 0$, 2, 4, and 8 V at $I = 0.1$ μA. (a–d) Schematic of $\Delta\sigma_{xx}$ as a function of B for temperatures ranging from 500 mK to 30 K. Solid lines represent fits to the HLN model. (e–h) Temperature dependence of L_ϕ, L_i, and L_*. (i–l) Temperature dependence of L_ϕ^{-2} on a double-logarithmic scale. The arrow points out the threshold temperature $T_{th} = 4$ K, above which the linear fit is performed. The linear fit yields the exponent p' which gradual decrease from ≈ 1 to ≈ 0.75 with increasing V_G. Error bars are the standard deviation (1σ) obtained from the linear fitting. (i) At $V_G = 0$ V, a linear fit (red line) yields an exponent $p' = 0.99 \pm 0.03$, which shows consistency with the dominant *e–e* scattering regime.. (For interpretation of the references to color in this figure legend, the reader is referred to the web version of this article.)

The three extracted characteristic lengths, L_ϕ, L_i, and L_*, are shown in Fig. 6e–h, at $V_G = 0$, 2, 4, and 8 V. Notably, the length of L_ϕ surpasses L_i and L_*, indicating that phase coherence persists over a longer length scale than intervalley and intravalley scattering processes. Moreover, L_i and L_* remain nearly temperature-independent across the entire measured temperature range and all investigated V_G. These results are consistent with previous studies [30,47].

The temperature dependence of the converted dephasing length L_ϕ^{-2} is presented in Fig. 6i–l on a double-logarithmic scale. Notably, the threshold temperature $T_{th} = 4$ K, as shown in Fig. 6i–l, is in good agreement with the threshold of the effective temperature $T_{eff\_th} = 4.05$ K, as shown in Fig. 4, indicating that the heating power required to overcome the energy relaxation via *e–p* scattering is consistent between current-heating and temperature-dependent measurements.

At $V_G = 0$ V (Fig. 6i), in the high-temperature regime ($T \geq 4$ K), L_ϕ^{-2} follows a clear power-law dependence, $L_\phi^{-2} \propto T^{p'}$, yielding an exponent $p' = 0.99 \pm 0.03$. This value is consistent with *e–e* scattering governed by the Nyquist mechanism in the dirty limit of two-dimensional systems [21–25], indicating that *e–e* scattering dominates the dephasing process in this temperature range with a low current applied ($I = 0.1$ μA).

A decrease from $p' \approx 1$ to ≈ 0.75, with increasing V_G, is explicitly shown in Fig. 6i–l. Although the fitted values carry finite uncertainties, both the upper and lower bounds of p' exhibit the same monotonic decrease with increasing V_G, supporting the robustness of the observed evolution. This evolution cannot be explained solely by a simple inclusion of *e–p* scattering, which results in a value of $p' = 1.5$ (Ref. [48,49]). Here, we consider two possibilities that might lead to the decrease of p'.

Firstly, we note that for a two-dimensional (2D) electron system dominated by Nyquist *e–e* interaction, one typically obtains a linear temperature dependence, corresponding to $p' = 1$. In contrast, for a one-dimensional (1D) diffusive system, Nyquist dephasing predicts a weaker temperature dependence, giving $p' = 2/3$ [21]. However, we do not expect such a dimensional crossover in the present devices, since the epitaxial graphene used in this study is a conventional Hall-bar geometry with a continuous two-dimensional conducting channel. We therefore consider a dimensionality reduction to be an unlikely explanation.

Secondly, we attribute the evolution to the increase in n with increasing V_G (see Fig. 3a), which leads to an enhancement in the density of states at the Fermi level, resulting in a stronger screening of the Coulomb interaction [49,50]. This suppresses the contribution from low-energy-transfer Nyquist scattering processes, which are inherently sensitive to long-range Coulomb interactions, dominating in the diffusive regime. Consequently, the phase-breaking rate deviates from the conventional situation, where $p' = 1$, and results in a smaller p' value. We note that the measured increase in n provides direct experimental support for this interpretation. Nevertheless, the present explanation is qualitative rather than a quantitative predictive model linking the screening strength to the extracted dephasing exponent p'. Nevertheless, the countering evolution of and the discrepancy between p and p' highlight that the equivalence between p and p' is not universal and should be carefully considered under different circumstances.

4. Conclusion

In conclusion, we demonstrate experimental evidence which indicates that the commonly assumed equivalence between p and p' may not hold beyond the current limit (≈ 0.5 μA) due to the nonequilibrium between *e–e* and *e–p* scattering processes. Furthermore, with increasing V_G, p increases from ≈ 2 to ≈ 3, indicating a crossover from *e–e* to *e–p* dominated energy relaxation, while p' decreases from ≈ 1 to ≈ 0.75, revealing a deviation from the conventional *e–e* diffusive dephasing picture. This contrasting evolution clearly exhibits that energy relaxation and phase coherence are governed by distinct microscopic processes and cannot be considered equivalent, especially under carrier-density tuning and hot-carrier conditions. Our results provide the necessity of

independently characterizing energy relaxation and phase coherence, and offer new insight into the interplay of scattering mechanisms in low-dimensional quantum systems. Notably, we acknowledge that this interesting evolution is reported in a single gated graphene on SiC, further work is required in order to substantiate our interpretation.

CRediT authorship contribution statement

Wei-Chen Lin: Writing – review & editing, Writing – original draft, Formal analysis, Data curation, Conceptualization. **Po-Shao Lai:** Writing – original draft, Formal analysis, Data curation. **Sung-Chieh Chiu:** Writing – original draft, Formal analysis, Data curation. **Pin-Chi Liao:** Writing – review & editing, Formal analysis. **Fa-Hua Chen:** Writing – review & editing, Formal analysis, Data curation. **Ji-Song Hsu:** Writing – review & editing, Data curation. **Ying-Je Wu:** Writing – review & editing, Formal analysis, Data curation. **Kenji Watanabe:** Writing – review & editing, Resources, Methodology. **Takashi Taniguchi:** Writing – review & editing, Resources. **Shao-Yu Chen:** Writing – review & editing, Supervision, Resources. **Albert F. Rigosi:** Writing – review & editing, Supervision, Resources, Funding acquisition. **Yanfei Yang:** Writing – review & editing, Supervision, Resources, Funding acquisition. **Chi-Te Liang:** Writing – review & editing, Writing – original draft, Supervision, Funding acquisition.

Declaration of competing interest

The authors declare that they have no known competing financial interests or personal relationships that could have appeared to influence the work reported in this paper.

Acknowledgments

C.-T. L. acknowledges support by National Science and Technology Council (NSTC), Taiwan (Grant No. NSTC 113-2112-M-002-034-MY3, and NSTC 115-2811-M-002-020) for financial support. S.-Y. C. acknowledges support by National Science and Technology Council (NSTC), Taiwan (Grant No. NSTC 114-2628-M-002-004) and Yushan Fellow Program by the Ministry of Education (MOE) (Grant No. NTU-114V1050-2) for financial support. K.W. and T.T. acknowledge support from the CREST (JPMJCR24A5), JST and World Premier International Research Center Initiative (WPI), MEXT, Japan. Commercial equipment, instruments, and materials are identified in this paper to specify the experimental procedure adequately. Such identification is not intended to imply recommendation or endorsement by National Institute of Standards and Technology or the United States Government, nor is it intended to imply that the materials or equipment identified are necessarily the best available for the purpose.

Work presented herein was performed, for a subset of the authors, as part of their official duties for the United States Government and funding is hence appropriated by the United States Congress directly.

Appendix A. Supplementary data

Supplementary material related to this article can be found online at https://doi.org/10.1016/j.carbon.2026.121956.

References

[1] K.C. Fong, K.C. Schwab, Phys. Rev. X 2 (2012) 031006.
[2] W.-K. Tse, S. Das Sarma, Phys. Rev. B 79 (23) (2009) 235406.
[3] S.S. Kubakaddi, Phys. Rev. B 79 (7) (2009) 075417.
[4] J.K. Viljas, T.T. Heikkilä, Phys. Rev. B 81 (24) (2010) 245404.
[5] K. Huang, A.C. Balram, H. Fu, C. Guo, K. Watanabe, T. Taniguchi, J.K. Jain, J. Zhu, Phys. Rev. X 15 (3) (2025) 031023.
[6] A. Majumdar, N. Chadha, P. Pal, A. Gugnani, B. Ghawri, K. Watanabe, T. Taniguchi, S. Mukerjee, A. Ghosh, Nat. Phys. 21 (9) (2025) 1374–1379.
[7] P.A. Lee, T.V. Ramakrishnan, Rev. Modern Phys. 57 (2) (1985) 287.
[8] T. Machida, H. Hirai, S. Komiyama, Y. Shiraki, Phys. Rev. B 54 (23) (1996) 16860.
[9] S. Koch, R.J. Haug, K. von Klitzing, K. Ploog, Semicond. Sci. Technol. 10 (2) (1995) 209–212.
[10] H.P. Wei, L.W. Engel, D.C. Tsui, Phys. Rev. B 50 (19) (1994) 14609.
[11] H. Scherer, L. Schweitzer, F.J. Ahlers, L. Bliek, R. Losch, W. Schlapp, Semicond. Sci. Technol. 10 (7) (1995) 959–964.
[12] A.K.M. Wennberg, S.N. Ytterboe, C.M. Gould, H.M. Bozler, J. Klem, H. Morkoc, Phys. Rev. B 34 (6) (1986) 4409.
[13] T. Brandes, L. Schweitzer, B. Kramer, Phys. Rev. Lett. 72 (22) (1994) 3582.
[14] E. Chow, H.P. Wei, S.M. Girvin, M. Shayegan, Phys. Rev. Lett. 77 (6) (1996) 1143.
[15] S. Koch, R.J. Haug, K.v. Klitzing, K. Ploog, Phys. Rev. Lett. 67 (7) (1991) 883.
[16] L.H. Willems van Beveren, D.L. Creedon, N. Eikenberg, K. Ganesan, B.C. Johnson, G. Chimowa, D. Churochkin, S. Bhattacharyya, S. Prawer, Phys. Rev. B 101 (11) (2020) 115306.
[17] G. Bergmann, Phys. Rep. 107 (1984) 1–58.
[18] J.-J. Lin, Phys. B 279 (1–3) (2000) 191–195.
[19] C.-C. Yeh, P.-C. Liao, D.K. Patel, W.-C. Lin, S.-C. Wang, A.F. Rigosi, R.E. Elmquist, C.-T. Liang, Phys. Rev. B 108 (20) (2023) 205304.
[20] J.-J. Lin, J. Bird, J. Phys.: Condens. Matter. 14 (18) (2002) R501–R596.
[21] B.L. Altshuler, A.G. Aronov, D.E. Khmelnitsky, J. Phys. C: Solid State Phys. 15 (36) (1982) 7367–7386.
[22] F.V. Tikhonenko, D.W. Horsell, R.V. Gorbachev, A.K. Savchenko, Phys. Rev. Lett. 100 (5) (2008) 056802.
[23] S. Pezzini, C. Cobaleda, E. Diez, V. Bellani, Phys. Rev. B 85 (16) (2012) 165451.
[24] R.V. Gorbachev, F.V. Tikhonenko, A.S. Mayorov, D.W. Horsell, A.K. Savchenko, Phys. Rev. Lett. 98 (17) (2007) 176805.
[25] W. Pan, A.J. Ross III, S.W. Howell, T. Ohta, T.A. Friedmann, C.-T. Liang, New J. Phys. 13 (11) (2011) 113005.
[26] B. Huckestein, Rev. Modern Phys. 67 (2) (1995) 357.
[27] D. Liu, S.D. Sarma, Phys. Rev. B 49 (4) (1994) 2677.
[28] F. Pierre, A. Gougam, A. Anthore, H. Pothier, D. Esteve, N.O. Birge, Phys. Rev. B 68 (8) (2003) 085413.
[29] H. Nakamura, D. Huang, J. Merz, E. Khalaf, P. Ostrovsky, A. Yaresko, D. Samal, H. Takagi, Nat. Commun. 11 (1) (2020) 1161.
[30] C.-C. Yeh, P.-C. Liao, Y. Yang, W.-C. Lin, A.R. Panna, A.F. Rigosi, R.E. Elmquist, C.-T. Liang, Phys. Rev. Lett. 133 (9) (2024) 096302.
[31] W.-C. Lin, C.-H. Yang, Y. Yang, C.-C. Yeh, P.-C. Liao, C.-W. Chang, R.E. Elmquist, C.-T. Liang, Carbon 244 (2025) 120702.
[32] Y. Yang, G. Cheng, P. Mende, I.G. Calizo, R.M. Feenstra, C. Chuang, C.-W. Liu, C.-I. Liu, G.R. Jones, A.R.H. Walker, R.E. Elmquist, Carbon 115 (2017) 229–236.
[33] A.F. Rigosi, M. Kruskopf, H.M. Hill, H. Jin, B.-Y. Wu, P.E. Johnson, S. Zhang, M. Berilla, A.R.H. Walker, C.A. Hacker, D.B. Newell, R.E. Elmquist, Carbon 142 (2019) 468–474.
[34] M. Musso, W.-C. Lin, Y. Yang, N.T.M. Tran, A.R. Panna, C.-H. Yang, R.E. Elmquist, D.B. Newell, C.-T. Liang, M. Ortolano, et al., IEEE Trans. Instrum. Meas. (2025).
[35] N.T.M. Tran, M. Musso, D. Scaletta, W.-C. Lin, V. Ortiz Jimenez, D. Jarrett, M. Ortolano, C. Richter, C.-T. Liang, D. Newell, et al., AIP Adv. 15 (8) (2025).
[36] A. Gupta, Y.J. Rho, W.-C. Lin, D.K. Patel, C.-T. Liang, M.K. Thakur, I. Kriegel, F.D. Stasio, S.H. Lee, Y.I. Park, J. Mater. Chem. A 13 (34) (2025) 28483–28495.
[37] N.T.M. Tran, M. Musso, D.S. Scaletta, W.-C. Lin, V.O. Jimenez, D.G. Jarrett, M. Ortolano, C.A. Richter, C.-T. Liang, D.B. Newell, et al., From wye-delta to cross-square recursion configurations in graphene-based quantum hall arrays, 2025, http://dx.doi.org/10.48550/arXiv.2508.03347, arXiv preprint arXiv:2508.03347.
[38] Supplementary Information.
[39] W. Norimatsu, Materials 16 (24) (2023) 7668.
[40] S. Tanabe, Y. Sekine, H. Kageshima, M. Nagase, H. Hibino, Phys. Rev. B 84 (11) (2011) 115458.
[41] V. Perebeinos, P. Avouris, Phys. Rev. B 81 (19) (2010) 195442.
[42] T. Machida, S. Komiyama, Phys. B 298 (1–4) (2001) 101–105.
[43] T. Machida, S. Komiyama, Phys. Rev. B 62 (19) (2000) 13004.
[44] F.-H. Liu, C.-S. Hsu, C. Chuang, T.-P. Woo, L.-I. Huang, S.-T. Lo, Y. Fukuyama, Y. Yang, R.E. Elmquist, C.-T. Liang, Nanoscale Res. Lett. 8 (1) (2013) 360.
[45] E. McCann, K. Kechedzhi, V.I. Fal'ko, H. Suzuura, T. Ando, B.L. Altshuler, Phys. Rev. Lett. 97 (14) (2006) 146805.
[46] Y. Yang, K.H. Gao, W.J. Wang, G. Yu, Y. Sun, X.H. Zhang, Z.Q. Li, Carbon 184 (2021) 287–294.
[47] D.-K. Ki, D. Jeong, J.-H. Choi, H.-J. Lee, K.-S. Park, Phys. Rev. B—Condens. Matter Mater. Phys. 78 (12) (2008) 125409.
[48] M. Očko, S. Žonja, G.L. Nelson, J.K. Freericks, L. Yu, N. Newman, J. Phys. D: Appl. Phys. 43 (44) (2010) 445405.
[49] A. Schmid, Z. Phys. 271 (3) (1974) 251–256.
[50] E.H. Hwang, S. Das Sarma, Phys. Rev. B 75 (20) (2007) 205418.